

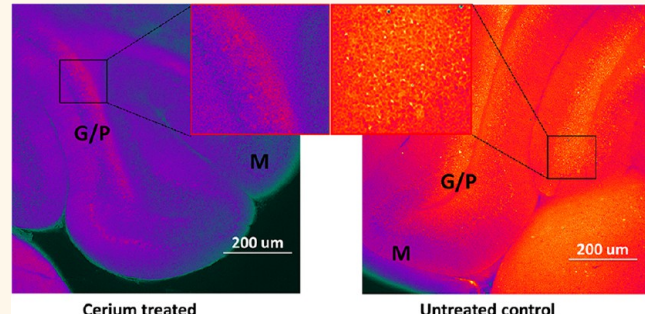
# Custom Cerium Oxide Nanoparticles Protect against a Free Radical Mediated Autoimmune Degenerative Disease in the Brain

Karin L. Heckman,<sup>†,▽,\*</sup> William DeCoteau,<sup>‡,▽</sup> Ana Estevez,<sup>†</sup> Kenneth J. Reed,<sup>§</sup> Wendi Costanzo,<sup>§</sup> David Sanford,<sup>§</sup> James C. Leiter,<sup>†</sup> Jennifer Clauss,<sup>†</sup> Kylie Knapp,<sup>†</sup> Carlos Gomez,<sup>†</sup> Patrick Mullen,<sup>†</sup> Elle Rathbun,<sup>†</sup> Kelly Prime,<sup>†</sup> Jessica Marini,<sup>†</sup> Jamie Patchefsky,<sup>†</sup> Arthur S. Patchefsky,<sup>||</sup> Richard K. Hailstone,<sup>#</sup> and Joseph S. Erlichman<sup>†</sup>

<sup>†</sup>Departments of Biology and <sup>‡</sup>Psychology, St. Lawrence University, Canton, New York 13617, United States, <sup>§</sup>Cerion Enterprises, LLC, Rochester, New York 14610, United States, <sup>†</sup>Department of Physiology and Neurobiology, Geisel School of Medicine at Dartmouth, Lebanon, New Hampshire 03756, United States,

<sup>||</sup>Department of Pathology, Fox Chase Medical Center, Temple Health, Philadelphia, Pennsylvania 19111, United States, and <sup>#</sup>Chester F. Carlson Center for Imaging Science, Rochester Institute of Technology, Rochester, New York 14623, United States. <sup>▽</sup>Both authors contributed equally to this work.

**ABSTRACT** Cerium oxide nanoparticles are potent antioxidants, based on their ability to either donate or receive electrons as they alternate between the +3 and +4 valence states. The dual oxidation state of ceria has made it an ideal catalyst in industrial applications, and more recently, nanoceria's efficacy in neutralizing biologically generated free radicals has been explored in biological applications. Here, we report the *in vivo* characteristics of custom-synthesized cerium oxide nanoparticles (CeNPs) in an animal model of immunological and free-radical mediated oxidative injury leading to neurodegenerative disease. The CeNPs are 2.9 nm in diameter, monodispersed and have a -23.5 mV zeta potential when stabilized with citrate/EDTA. This stabilizer coating resists being 'washed' off in physiological salt solutions, and the CeNPs remain monodispersed for long durations in high ionic strength saline. The plasma half-life of the CeNPs is ~4.0 h, far longer than previously described, stabilized ceria nanoparticles. When administered intravenously to mice, the CeNPs were well tolerated and taken up by the liver and spleen much less than previous nanoceria formulations. The CeNPs were also able to penetrate the brain, reduce reactive oxygen species levels, and alleviate clinical symptoms and motor deficits in mice with a murine model of multiple sclerosis. Thus, CeNPs may be useful in mitigating tissue damage arising from free radical accumulation in biological systems.



**KEYWORDS:** nanoparticles · free radicals · experimental autoimmune encephalitis · tissue distribution · blood brain barrier

**N**anocrystalline cerium oxide is widely studied as a multifunctional material used in myriad industrial and manufacturing processes including catalysis, fuel cells, polishing agents, and combustion adjuvants. The ability of nanoceria to participate in redox coupled reactions has made these nanoparticles attractive candidates for development in biological and medical applications,<sup>1–6</sup> and recent studies have focused on the biological outcomes of administering cerium oxide nanoparticles to experimental animals using disease models in which free radicals are thought to play a prominent role.<sup>1,2,7</sup>

Cerium is a lanthanide element with a crystalline structure that can exist in two oxidation states ( $\text{Ce}^{3+}$  or  $\text{Ce}^{4+}$ ), which can be interchanged depending on the redox environment within biological systems.<sup>5,8,9</sup> The catalytic properties of ceria have been attributed to the presence of highly mobile lattice oxygen present at the surface,<sup>10–13</sup> which facilitates the  $\text{Ce}^{4+} \rightarrow \text{Ce}^{3+}$  conversion and is correlated with decreased free radical levels.<sup>13</sup> The redox reactivity of cerium oxide nanoparticles *in vitro* has been studied extensively.<sup>14–21</sup> The half-cell potential of ceria nanoparticles falls between the redox potential of superoxide, hydroxyl ion and

\* Address correspondence to kheckman@stlawu.edu.

Received for review June 4, 2013 and accepted November 22, 2013.

Published online November 22, 2013  
10.1021/nn403743b

© 2013 American Chemical Society

peroxynitrite (all have lower half-potentials) and hydrogen peroxide (half-cell potential =  $-1.7$  V). Thus, ceria is well positioned to oxidize biologically important reactive oxygen and nitrogen species with lower half-potentials, such as superoxide and peroxynitrite. Further, nanoceria catalyze the same electron transfer reactions as superoxide dismutase, catalase and glutathione.<sup>22</sup> The regenerative oscillation between valence states suggests that nanoceria may have value as a therapeutic agent in the treatment of diseases related to the accumulation of reactive oxygen species (ROS).<sup>3,4</sup> However, the majority of studies have used reduced preparations to study cellular effects *in vitro*, which, despite providing important insight into the mechanisms of action of the particles, do not fully recapitulate the biological interactions *in vivo*.<sup>5–7,23–27</sup>

The studies of ceria function *in vivo* used nanoceria ranging in size from 5 to 55 nm,<sup>1,2,7,28</sup> often with negative zeta potentials ( $<-50$  mV), administered as dispersions or nominally stabilized with citrate or polyethylene glycol.<sup>2,29</sup> In rodent models, these particles were prone to aggregate and accumulate in the spleen and liver.<sup>1,29–31</sup> This pattern of tissue distribution is characteristic of 'bare' nanoparticles and nanoparticles that have not been adequately stabilized. In either case, excess deposition in the liver may result in toxicity at higher doses.<sup>32–34</sup> Nanoceria in the previously described formulations did not readily cross the blood brain barrier (BBB),<sup>31,32,35</sup> and these formulations have promoted oxidative stress in some settings.<sup>32</sup> Discrepancies among the biological effects of various nanoceria formulations have been attributed to many factors including synthetic routes, composition/purity, particle size and surface charge.<sup>3,4,36</sup> Unfortunately, none of these characteristics, *a priori*, have been particularly helpful in evaluating biological outcomes, which suggests that the interaction of the particles with proteins in different cellular compartments may provide more useful insight into biological differences among formulations.

Clearance of nanoceria from the body is another point of concern. The nanoparticles are taken up by the resident macrophages of the liver, the Kupfer cells.<sup>29</sup> In previous *in vivo* studies, administration of unstabilized, bare or citrate-stabilized ceria nanoparticles was associated with high accumulation in the reticuloendothelial organs, tissue toxicity and poor tissue clearance rates,<sup>29,34</sup> all of which suggest that additional surface functionalization/stabilization may be required before ceria nanoparticles can be developed for therapeutic applications. To this end, our group has synthesized unique cerium oxide nanoparticles (CeNPs) with characteristics distinct from commercially available particles and those used by other groups.

Our custom CeNPs were synthesized by a novel process that generates smaller, highly uniform (2.9 nm) particles with a less negative zeta potential, and the

particles were treated with a stabilizer comprised of citrate and EDTA, which resists 'washing' off in physiological solutions.<sup>37</sup> EDTA seems to alter the surface potential of the particle and provides a durable coating by binding to the ceria. Citrate may act as an electron transfer agent between the particle and reactive oxygen species that reside in the oxygen vacancies on the surface of the nanoceria crystal. Here, we describe the biological effects of administering our unique CeNPs in a murine model of multiple sclerosis, experimental autoimmune encephalomyelitis (EAE). Oxidative stress generated by immune cells plays a significant role in this autoimmune and neurodegenerative disease, which results in the loss of motor function and impaired limb movement in affected animals. Intravenous delivery of CeNPs reduced clinical disease severity and improved motor function compared to control animals when the particles were delivered in both preventative and therapeutic treatment regimens. CeNP-treated animals also exhibited reduced ROS levels in the brain following drug administration, demonstrating that the nanoparticles retained antioxidant properties and may be promising candidates for further development in the treatment of oxidative injury.

## RESULTS

**Characterization of Custom-Synthesized CeNPs.** After synthesis, the solution containing the CeNPs was clear and yellow and displayed Tyndall scattering when illuminated with a low intensity laser, indicating that the solution contained well-dispersed colloidal particles. Figure 1 shows transmission electron microscopy (TEM) (a) and electron diffraction (ED) images (c) of the CeNP material. The diffraction pattern is consistent with a fluorite lattice structure of  $\text{CeO}_2$ ; the most intense line (111) corresponds to 0.312 nm lattice spacing as expected for the fluorite structure of  $\text{CeO}_2$ . Results of X-ray diffraction performed on dried particles corroborated the fluorite structure. The nanoparticles consisted of single 2.4 nm crystallites of cerium dioxide (Figure 1D). In water, the average hydrodynamic diameter of the particles was  $2.9 \pm 0.3$  nm (Figure 1B) with a polydispersity of  $0.19 \pm 0.03$ , based on dynamic light scattering (DLS) measurements (Figure 1D). The zeta potential of the final particle was  $-23.5 \pm 1.3$  mV. The material did not change size when stored at room temperature for up to two years after synthesis, and repeated, high-speed centrifugation (100 000g, 4 °C for 3 h) failed to pellet the material or significantly change its size as determined by DLS analysis.

**CeNP Size in High Ionic Strength Solutions.** To evaluate the likelihood of CeNP aggregation in high ionic strength solutions that mimic biological solutions, our custom synthesized CeNPs were placed in simulated body fluid (SBF; 1:1 dilution by volume;  $\sim 305$  mOsm)

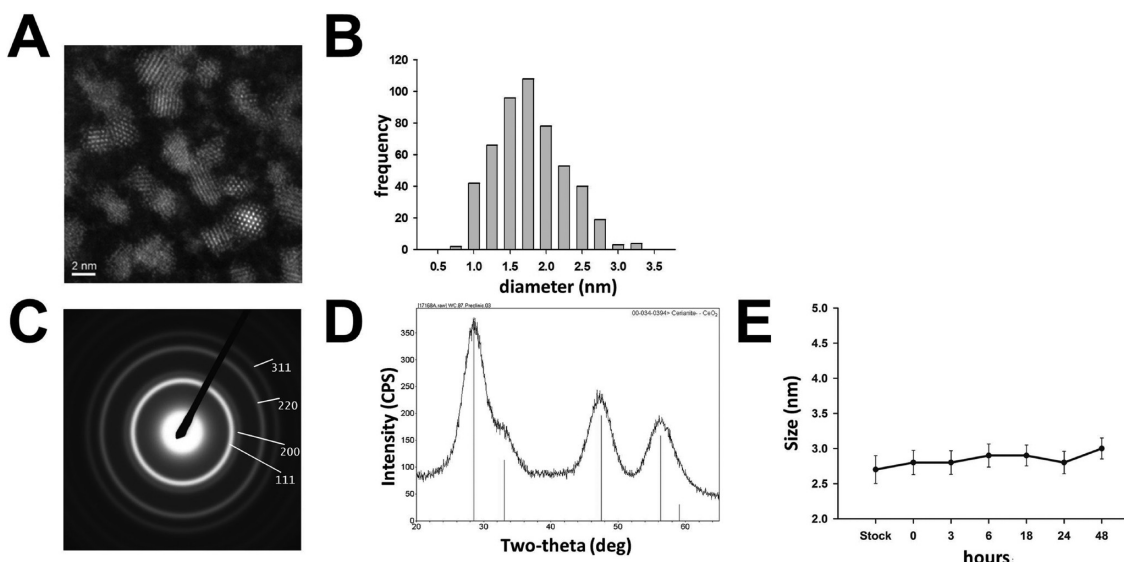


**Figure 1. Characterization of custom-synthesized CeNPs.** CeNPs were imaged by TEM (A), and their size distribution is shown in (B). Electron diffraction analysis of CeNPs (C) demonstrated the presence of ceria, while X-ray diffraction (D) identified the crystalline structure. CeNPs were added to simulated body fluid, and their size was determined over a 48 h period using DLS (E). High ionic strength solutions had little effect on agglomeration and size.

for 48 h, and the size of the particles was measured periodically using dynamic light scattering. Once the solution was diluted in the physiological saline, the size of the CeNPs was unchanged relative to the stock solution and remained monodispersed for up to 48 h (Figure 1E).

**Plasma Half-Life and Clearance of CeNPs in Healthy Animals.** Next we evaluated the plasma clearance of the CeNPs when delivered *in vivo*. The plasma half-life of the CeNPs (10 mg/kg intravenous dose) was  $\sim$ 3.7 h with a mean residence time of 5.4 h in Sprague–Dawley rats (Figure 2A). To evaluate tissue clearance, healthy mice ( $n = 10$ ) were injected with a single, intravenous dose of CeNPs (20 mg/kg), and ceria content was measured at different time points. Tissues were harvested 24 h later to determine the initial loading dose of ceria in various organs. CeNPs were detected by inductively coupled mass spectroscopy (ICP-MS), and the highest tissue levels were measured in the liver (Figure 2B) and spleen (Figure 2C), followed by the kidney (Figure 2E) and the brain (Figure 2D). Over time, the ceria levels in the liver and brain declined continually, and low levels of ceria were retained even 5 months after administration (Figure 2B,D). CeNP levels in the spleen and kidney initially rose after the loading levels were achieved, peaked at 1–2 months postadministration and then declined (Figure 2C,E). In contrast to the other organs, the CeNP content in the spleen decreased after 3 months only to approximately the level present at the loading stage. It is noteworthy that measurable brain levels of ceria were detected even in these healthy mice with intact BBBs.

**Application of CeNPs to a Murine Model of Oxidative Stress.** We sought to observe whether the CeNPs retained their antioxidant capabilities using an *in vivo*

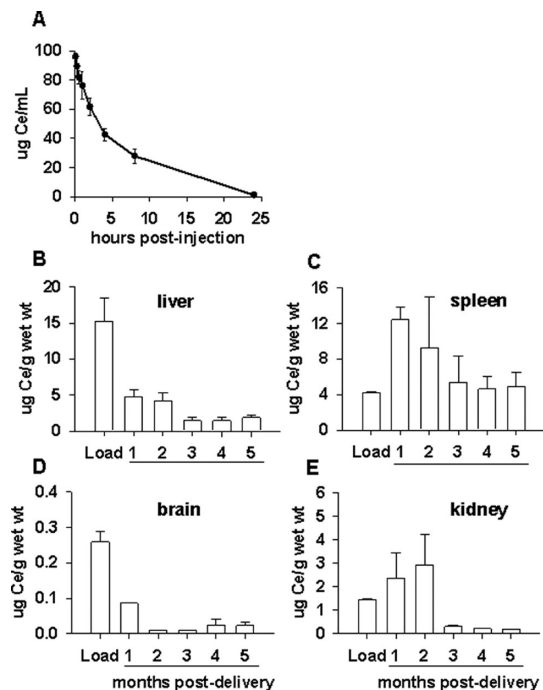


**Figure 2. CeNP half-life and tissue clearance.** (A) A total of 10 mg/kg of CeNPs was administered intravenously to healthy Sprague–Dawley rats, and blood was collected over a 24 h period. Ceria content was measured by ICP-MS. (B–E) Healthy SJL/J mice were injected with one intravenous 20 mg/kg CeNP dose, and various tissues were harvested 24 h (Load 1) or 1, 2, 3, 4, or 5 months postadministration. Liver (B), spleen (C), brain (D), and kidney (E) tissues were analyzed by ICP-MS for ceria content expressed as micrograms of Ce per gram of tissue wet weight ( $\mu\text{g Ce/g wet wt}$ ).

disease model. Given the efficacy of the CeNPs in neutralizing a variety of free radicals *in vitro*<sup>22</sup> and their distribution to the brain *in vivo*, a central nervous

**TABLE 1. Sample Size for Each CeNP Dose and Treatment Regimen<sup>a</sup>**

	CeNPs		
	10 mg/kg	20 mg/kg	30 mg/kg
<b>Preventative:</b> 15 mg/kg the day before and day of induction, on day 3, followed by maintenance dose at right	<i>n</i> = 13	<i>n</i> = 12	<i>n</i> = 15
<b>Therapeutic 3 day delay:</b> first dose day 3 after induction then maintenance dosing	<i>n</i> = 15	<i>n</i> = 17	
<b>Therapeutic 7 day delay:</b> maintenance dosing only			<i>n</i> = 15
<b>Control:</b> vehicle control injections	<i>n</i> = 15	<i>n</i> = 15	<i>n</i> = 15
<b>Fingolimod:</b> provided continuously beginning day 7 after induction			<i>n</i> = 15

<sup>a</sup> CeNPs and control solutions were delivered in 100  $\mu$ L volume intravenously. Maintenance doses were given every 7 days after induction through day 35.

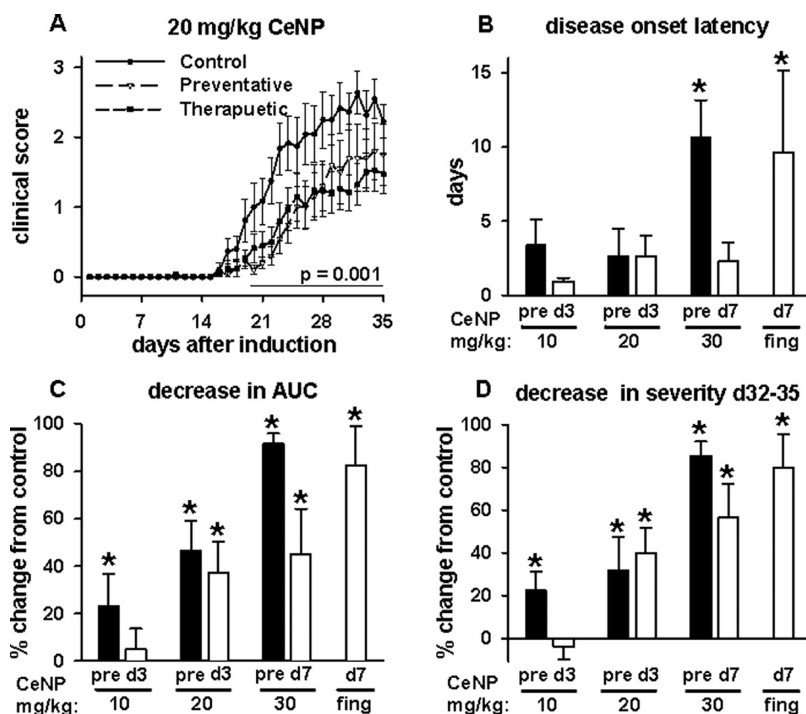


**Figure 3. CeNP treatment delays disease onset and alleviates disease severity of EAE.** (A) The temporal pattern of disease severity following induction of EAE with MOG<sub>35–55</sub> in mice receiving 20 mg/kg CeNPs in a preventative and therapeutic (3 day) regimen (see Table 1) and in the matched control group. Delay in disease onset (B) and disease severity (AUC expressed as a percent of the value in control animals) (C) are shown as a function of CeNP dose (10, 20, or 30 mg/kg) and administration regimen. (D) Mean disease severity during the last 4 days of treatment is shown as a function of the CeNP dose (10, 20, or 30 mg/kg) and administration regimen. For (B–D), black bars indicate preventative CeNP treatment regimens, while white bars indicate therapeutic treatment regimens of either CeNPs or fingolimod. pre: preventative CeNP regimen. d3: day 3 therapeutic CeNP regimen. d7: fingolimod or 30 mg/kg CeNP treatment started 7 days after induction of EAE. fing: fingolimod. Asterisk (\*) indicates  $p < 0.05$  compared to control animals.

system (CNS) disease involving oxidative damage was selected for study. Multiple sclerosis (MS) is a chronic, immunological and neurodegenerative disease characterized by degradation of neuronal myelin sheaths and, at times, neuronal death, resulting in impaired nerve impulse conduction and, ultimately, cognitive and motor dysfunction in affected patients.<sup>38</sup> The cellular mediators of disease include macrophages that invade the brain<sup>39</sup> and produce reactive oxygen species.<sup>38</sup> Superoxide anions, peroxynitrite and hydrogen peroxide participate in disruption of the BBB in MS<sup>40</sup> and also oxidize DNA, proteins and lipids, damage that can induce genomic instability and the death of neurons.<sup>41</sup> We studied a murine model of MS, experimental autoimmune encephalomyelitis (EAE),

hypothesizing that administration of the CeNPs would reduce levels of free radicals and alleviate disease severity in this well-characterized animal model.

Chronic progressive EAE was induced in C57BL/6 mice using the MOG<sub>35–55</sub> peptide. A variety of CeNP doses and dosing regimens were tested (Table 1), and these results were compared with the effectiveness of the immunomodulatory agent fingolimod, which is currently used to treat patients with relapsing MS and which we used to benchmark the effectiveness of CeNP treatments.<sup>42</sup> Clinical scores, which take into account limb mobility, were assigned as a metric of disease severity. A typical example of EAE disease progression is depicted in Figure 3A, and the mean clinical scores of animals treated preventative or

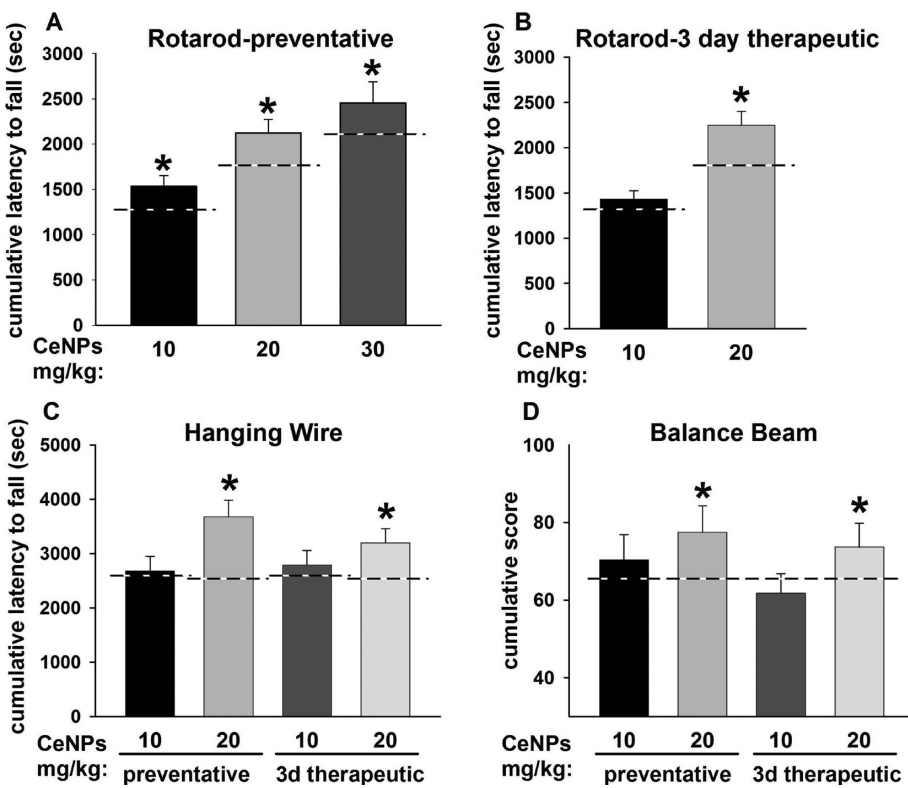


**Figure 4.** Treatment with CeNPs improves motor function of animals with EAE. (A and B) The cumulative latency to fall on the rotarod test (calculated as AUC) in each animal is expressed as a function of the CeNP dose (10, 20, or 30 mg/kg) and preventative (A) or 3 day therapeutic (B) administration regimen. Cumulative latency to fall on the hanging wire test (calculated as AUC) (C) and cumulative balance beam score (D) of each animal are also expressed as a function of the dose (10, 20, or 30 mg/kg) and administration regimen. Dashed lines indicate the mean (rotarod and hanging wire tests) or median (balance beam test) scores of the matched control animals at each dose of CeNPs studied. sec: seconds. Other abbreviations and symbols are as described in Figure 3.

therapeutically with 20 mg/kg CeNPs are compared with those of control animals. Both of the CeNP dosing regimens were associated with significantly reduced disease severity compared to control treatment starting approximately 19 days after EAE induction ( $p < 0.001$ ). Average responses for all treatment groups are summarized in Figure 3B–D. EAE onset was significantly delayed by the preventative 30 mg/kg CeNP dose and by fingolimod treatment (Figure 3B). In all dosing paradigms except the 10 mg/kg therapeutic 3 day delay regimen, CeNP treatment significantly decreased total disease severity (measured as the area under the curve of clinical scores days 0–35; Figure 3C). Fingolimod also significantly reduced total disease severity, and the efficacy of preventative treatment with 30 mg/kg CeNPs was similar to the efficacy of fingolimod. Since this EAE model mimics a chronic (nonrelapsing) form of MS, we examined the durability of the treatment effects by assessing the average clinical scores in the last four days (days 32–35) of the experiment. Clinical scores during this late phase of disease were significantly reduced at most CeNP doses compared to control treatment ( $p \leq 0.045$ ), including the therapeutic 7 day delay group that received 30 mg/kg CeNPs (Figure 3D). Further, the higher doses of CeNPs

were as effective as, and not significantly different from, the late response to fingolimod treatment ( $p > 0.05$ ).

**Effect of CeNP Treatment on Motor Function.** Though the manifestations of EAE generally develop in a caudal to rostral direction,<sup>43</sup> the clinical scoring scale is dominated by caudal motor function. Since we were concerned that subtle improvements in motor activity in rostral motor groups might be missed by this metric, we performed specific tests of motor function to assess the effects of CeNP treatment more completely: rotarod (mainly caudal function), hanging wire (rostral function only), and balance beam (both caudal and rostral function). Predisease performance did not differ among treatment groups ( $p > 0.1$ ), and with the exception of the 10 mg/kg dose, preventative CeNP administration yielded higher latencies to fall in the rotarod and hanging wire tasks and improved balance beam scores compared to the effects of the delayed, therapeutic dosing regimen (Figure 4). This finding could be either the result of differences in the timing of drug delivery or the cumulative dose administered (animals treated earlier also received a larger cumulative dose of CeNPs). Within a dosing regimen (*i.e.*, preventative or therapeutic), a significant CeNP dose–response effect was observed for all motor tests;

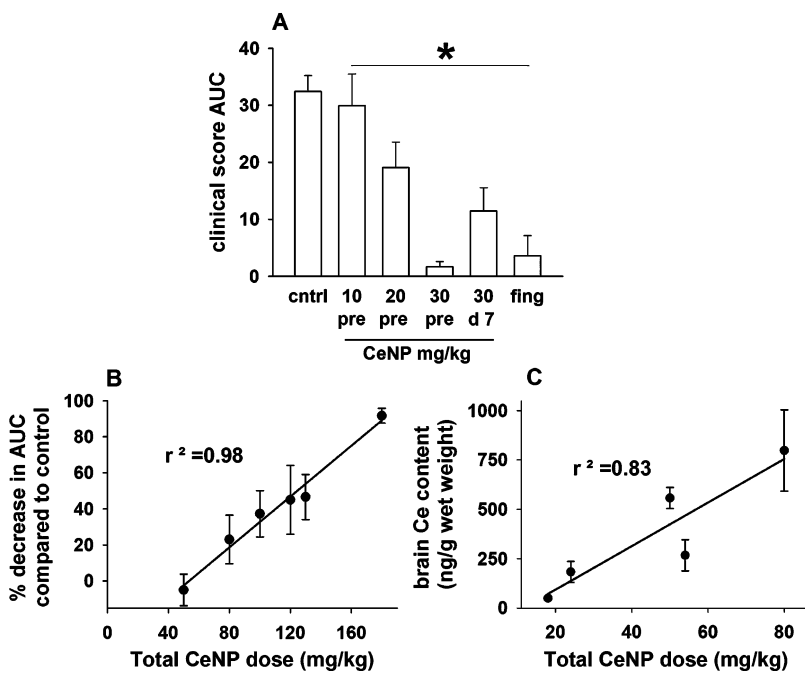


**Figure 5.** EAE clinical scores improve in a dose-dependent manner with CeNP treatment and tissue deposition. (A) Cumulative EAE severity (calculated as AUC) was proportionately reduced with increasing CeNP treatment dose. The 30 mg/kg CeNP dose yielded disease protection similar to that of the fingolimod treatment, regardless of when the CeNP treatment was started. The decrease in cumulative disease severity compared to control animals (B) and deposition of CeNPs in the brain (C) are expressed as a function of the cumulative dose of ceria given in each treatment group. Cerium content in the brain was analyzed by mass spectroscopy in a subset of animals; thus, the cumulative dose of ceria (x-axis) is not equal in (B) and (C). Asterisk (\*) indicates that all treatment groups were significantly less than control ( $p < 0.05$ ). Abbreviations are as described in Figure 3.

higher doses of CeNPs preserved motor function more effectively in all tests (Figure 4).

**CeNP Dose Response Characteristics.** In general, cumulative disease severity (measured as AUC of clinical scores) was inversely related to the individual CeNP dose regardless of the timing of administration (Figure 5A). Expressing the reduction in disease severity as a function of the cumulative CeNP dose delivered demonstrated that, regardless of dosage timing, higher cumulative doses of CeNPs were significantly correlated with the reduction in the AUC of disease severity ( $r^2 = 0.98; p = 0.001$ ) (Figure 5B). Moreover, these effects may be attributable to brain penetration of the CeNPs, since tissue levels of CeNPs were well-correlated with the cumulative dose of CeNPs delivered ( $r^2 = 0.83; p = 0.03$ ) (Figure 5C). No plateau in the relationships between cumulative CeNP dose and either disease severity reduction or brain CeNP levels was observed, suggesting that the maximum therapeutic brain concentration of CeNPs was not reached in these experiments.

**Biodistribution of CeNPs in EAE Animals.** ICP-MS analysis of brain tissue indicated that multiple doses of CeNPs accumulated in the CNS, particularly in the cerebellum (Figure 6A), a region with significant damage in EAE animals.<sup>44</sup> Moreover, cerebellar ceria levels were approximately two times higher than in the spinal cord and the other brain regions (Figure 6A). Consistent with previous *in vitro* findings<sup>22</sup> and our mass

spectroscopy data, TEM analysis of the cerebellum of CeNP-treated animals revealed deposition of CeNPs throughout the intracellular compartments in myelinated processes, axons, dendrites and mitochondria (Figure 6B): sites of ROS production and targets of free radical damage. Though hepatic toxicity and particle aggregation have been observed after administration of other nanoparticle formulations in rodents,<sup>30,32–35</sup> we detected relatively low levels of CeNPs in the liver compared to the CNS (Figure 6A), and we found no evidence of liver pathology in CeNP-treated animals with cumulative doses as high as 130 mg/kg of CeNPs in the preventative treatment regimen. Both control and treatment groups showed mild focal portal lymphocytic infiltrates, and intracytoplasmic fat deposition was minimal, suggesting that these responses in the liver may have been related to disease induction as opposed to specific drug treatment effects.

**Durability of CeNPs' Mechanism of Action.** To test whether the CeNPs detected in the cerebellum retained their catalytic activity over time, ROS levels in the brains were assessed late in the EAE disease course (day 42). Fresh cerebellar brain slices were harvested from control, fingolimod or CeNP (preventative regimen 30 mg/kg dose) treated animals and stained with the free radical indicator dye, H<sub>2</sub>CMDCFDA, to provide an estimate of the total ROS load. ROS levels in tissues from the fingolimod and control treated animals did not differ significantly (Figure 7A;  $p = 0.619$ ), though

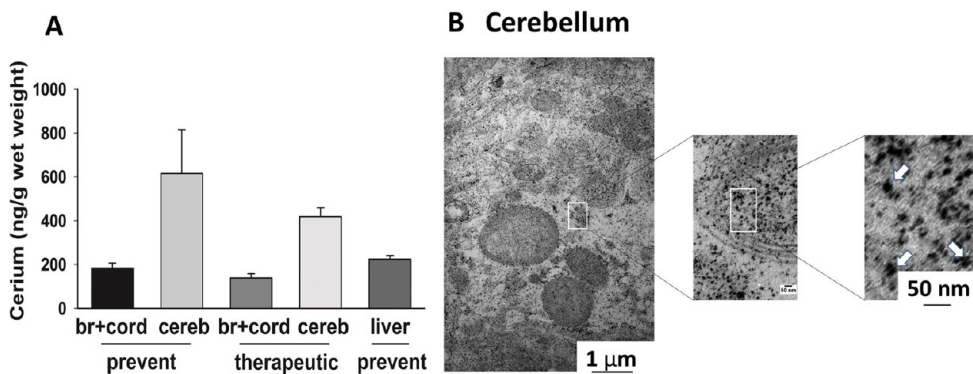


**Figure 6.** CeNP deposition in CNS tissues. (A) Tissues from EAE mice treated with 20 mg/kg CeNPs in preventative or therapeutic regimens were harvested from PBS-perfused animals and subjected to ICP-MS. Brain (without cerebellum) and spinal cord samples were pooled (br + cord) for analysis. (B) TEM images of the cerebellum of an EAE mouse treated with 30 mg/kg CeNPs (preventative regimen) are shown; note the dense black particles at the highest magnification. These particles were particularly prominent in mitochondria. Arrows indicate putative particles. cereb: cerebellum. prevent: preventative regimen.

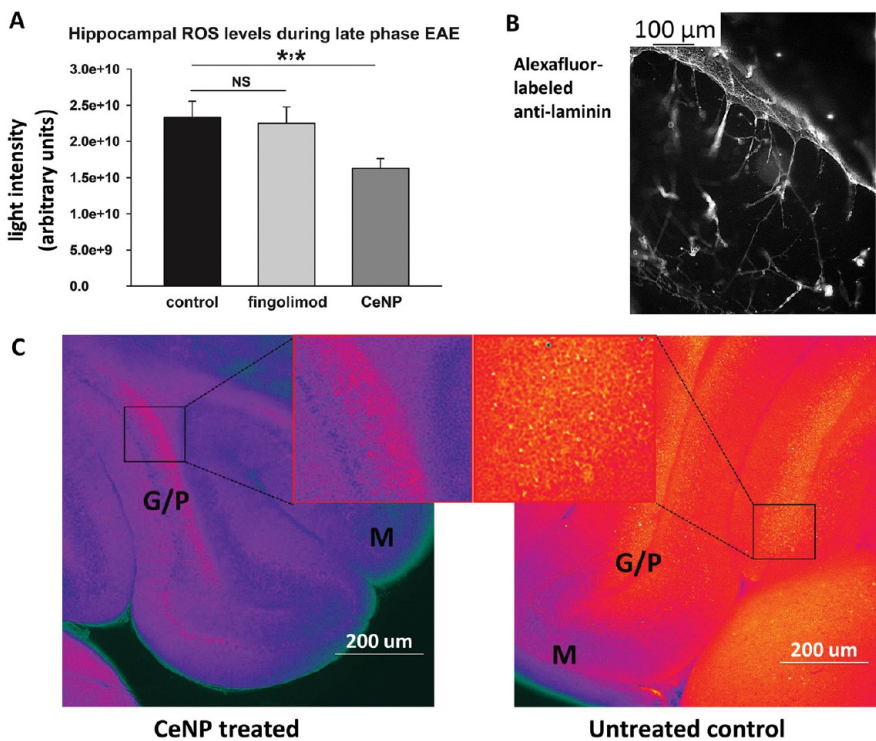


**Figure 7.** CeNPs decrease cerebellum ROS levels in EAE mice. (A) ROS levels were measured with a nonspecific free radical fluorophore (CM-H<sub>2</sub>DCFDA) in brain slices prepared from 30 mg/kg CeNP treated (preventative regimen) or fingolimod treated mice beginning on day 42 after induction of EAE. This time point fell at least 7 days after the last CeNP treatment. (B) The cerebellum was stained with an antilaminin AlexaFluor reagent to illustrate the location of the detected ROS staining (C) relative to vasculature in brain slices. (C) Representative images of ROS detected in brain slices from a CeNP treated animal (left) and a control animal (right), which was injected with saline only. G/P: granular/Purkinje layer; M: molecular layer.

ROS levels in tissues from CeNP treated mice were reduced by ~31% ( $p < 0.001$  compared to either control or fingolimod treated animals), indicating that the CeNPs retained their catalytic, antioxidant activity. The majority of the ROS signal was derived from cells located in the granular/Purkinje cell layers of the cerebellum (Figure 7C). The ROS signal was much lower in the surrounding molecular layer (suggesting that the ROS signal reflected the intrinsic ROS generation rate

of different types of neurons rather than nonspecific slice trauma). Moreover, immunohistochemical staining of the microvasculature (Figure 7B) showed an entirely different pattern of staining compared to the ROS staining, illustrating that intravenously administered CeNPs were not captured solely by endothelial cells, and that ROS were not being neutralized only in the vascular compartment of the brain. CeNP deposition extended far beyond vessel endothelial cells and

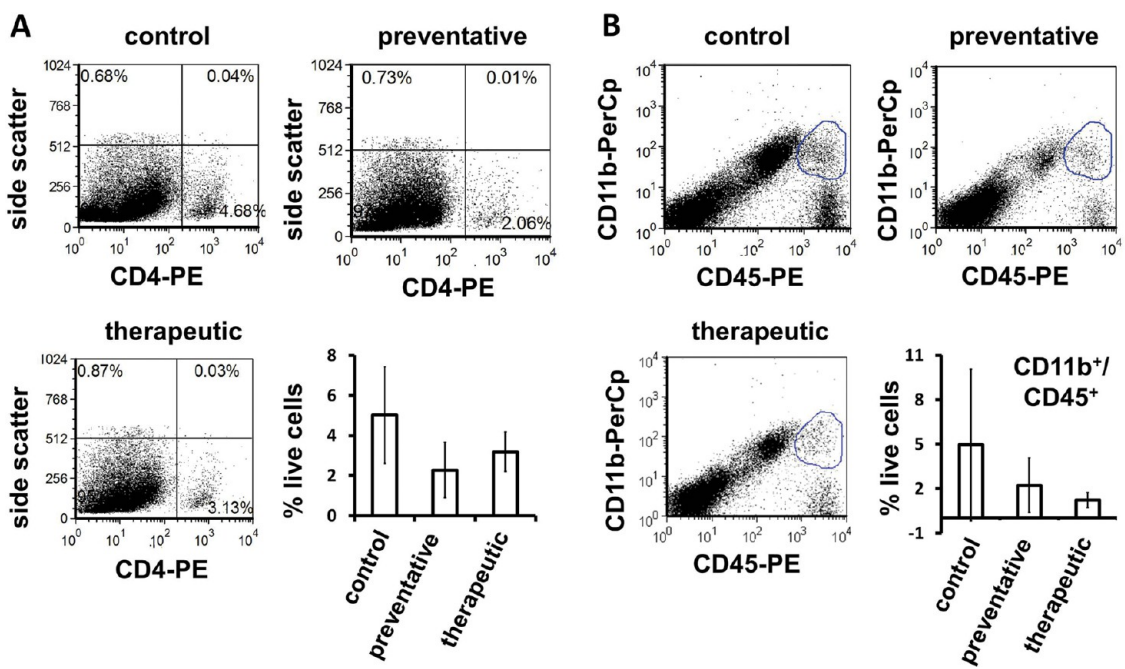


**Figure 8.** CeNP treatment does not modulate TH cell and macrophage populations in the brain. Brains of EAE animals treated with control or 10 mg/kg CeNPs were harvested on day 45. Cells from this homogenized tissue were stained for FACS analysis with anti-CD4 or a combination of anti-CD11b and anti-CD45 fluorochrome conjugated antibodies. Representative plots from each treatment group and compiled results are represented for each CD4<sup>+</sup> TH cells (A) and CD11b<sup>+</sup>/CD45<sup>+</sup> macrophages (B).

penetrated into the actual brain tissue (Figure 7B), consistent with the intraneuronal distribution of CeNPs in the TEM images (Figure 6B).

**Lack of Effect of CeNPs on Immune Cell Distributions.** Diminished ROS levels in the brains of CeNP-treated EAE animals implied that the ROS component of EAE pathology was therapeutically altered by CeNP treatment (Figure 7), which likely contributed to decreased disease severity (Figures 3 and 4). This efficacy is encouraging, given that the immune system might recognize nanomaterials as foreign antigens and mount an immune response against the CeNPs.<sup>45</sup> It seems unlikely that the CeNP-dependent improvements in clinical disease severity scores were derived from changes in T helper cell or macrophage function in the CNS, but we tested the possibility that CeNPs may ameliorate EAE by modulating immune cell function. We harvested the brains of EAE mice treated with 10 mg/kg CeNPs in preventative or therapeutic 3 day delay dosage regimens on day 45 (10 days after the last CeNP treatment). CD4<sup>+</sup> T helper cells and macrophages (CD11b<sup>+</sup> CD45<sup>+</sup> cells) were quantified using fluorescence-activated cell sorting (FACS). Levels of each cell type were lower in CeNP-treated animals compared to control animals (Figure 8). However, there was great variability within treatment groups, and the differences among the control, preventative and therapeutic groups were not statistically significant (CD4<sup>+</sup> T cells,  $p = 0.07$ ; macrophages,  $p = 0.195$ ). Thus, despite sustained biological activity and deposition of CeNPs in the brains of treated animals, immune cell infiltration

into the brain was not different among the treatment and control groups, and we have no evidence of immunomodulatory effects of CeNPs in this model of EAE, though we tested only the lowest dose of ceria nanoparticles that we studied.

## DISCUSSION

The CeNP formulation used in the current study differs from other cerium oxide nanoparticles in several important respects including size (2.9 nm), surface charge and the stabilizer bound to the surface of the particles (citrate/EDTA). These characteristics result in a particle that remains monodispersed in physiological solutions, resists agglomeration even when centrifuged, and has an extended plasma half-life approximately four times longer than previous ceria/citrate formulations of similar size.

Delivery of nanoceria to an intact biological system can yield changes to structure and function that are distinct from *in vitro* properties. When weakly stabilized or unmodified nanoceria enter the body, they interact with proteins, lipids and cells in a complex milieu with a high ionic strength. Interactions among the constituents of this milieu seem to modify the original nanoparticle surface, and a protein corona may form (*i.e.*, the Vroman Effect).<sup>46,47</sup> For many materials, the complement of proteins bound to the particle's surface results in significant deposition in the reticuloendothelial organs (*i.e.*, liver and spleen) and little opportunity for deposition in other tissues, in particular, the brain. Commercially available, unstabilized or

citrate-stabilized cerium oxide nanoparticles were deposited in the highest concentrations in the spleen and liver in rodents, where they were retained at high levels for up to 90 days.<sup>1,29–32</sup> In the present study, tissue levels of CeNPs in the liver and spleen were extremely low in healthy animals (Figure 2) compared to previous studies using 5 nm, citrate-stabilized nanoceria at similar time points. Moreover, the CeNP deposition in the liver of the animals with EAE (Figure 6A) was considerably lower than that in healthy mice, suggesting that disease state may influence nanoparticle distribution in the reticuloendothelial system. These deposition patterns are consistent with the notion that our CeNPs adsorbed fewer proteins that direct the particles to the reticuloendothelial system, and for this reason, our particles exhibited much longer circulation times (3.7 vs 1 h). The combination of citrate/EDTA, perhaps like PEG on other nanoparticles, seemed to reduce the association of proteins to the surface of the nanoceria.

The ceria content of the organs measured in the present study decreased below loading values, except in the spleen. This contrasts with previous reports that showed little decrease in tissue ceria content up to 3 months postinjection.<sup>29</sup> For example, using nonstabilized, 3–5 nm particles, Hirst *et al.* showed that a cumulative dose of 2.5 mg/kg delivered over a 5 week period resulted in the deposition of >20 000 µg/g of ceria in the liver and >30 000 µg/g in the spleen one week after the final injection.<sup>27</sup> In rats, a single 85 mg/kg injection of citrate-stabilized ceria (5 nm) resulted in 500 µg/g of ceria in the liver up to 90 days following the injection.<sup>32</sup> In a similar study using 30 nm citrate-stabilized ceria, Yokel *et al.* showed that a 70 mg/kg infusion resulted in ~1000 µg/g of nanoceria in the liver and spleen across the 3 month study.<sup>29</sup> Thus, nonstabilized nanoceria were retained in the reticuloendothelial system to a much greater extent than citrate-stabilized particles, regardless of particle size, and citrate/EDTA-stabilization resulted in the least deposition compared to other stabilizer formulations.

Frequent and rapid agglomeration of other nanoparticles in physiological salt solutions dictates that the nanomaterial be delivered in water. For many typical surface treatments used to condition nanoparticles (citrate, lactate, etc.), high ionic strength solutions seem to strip away the surface treatment, allowing the particles to aggregate, which reduces their biological activity. In contrast, the citrate/EDTA stabilized CeNPs were resistant to stabilizer loss in high ionic strength solutions, remained dispersed in solution and retained their small size for relatively long periods of time (Figure 1E). Following administration of nanoparticle formulations used by other groups, both the large size of the aggregates and the exposure of the particle surface may accelerate association with proteins in the body that promote deposition in the

reticuloendothelial system.<sup>48–50</sup> For example, the binding of complement proteins to nonstabilized nanoparticles promotes uptake and clearance of nanomaterials by circulating and tissue resident macrophages.<sup>51,52</sup> The presence or lack of stabilizer also correlates with plasma half-life: ~7 min for nonstabilized nanoceria and 1 h for citrate stabilized particles.<sup>30,31,53</sup> In contrast, the half-life of our CeNPs was 3.7 h, considerably longer than that of ceria stabilized with citrate alone. Treatment with a combination of citrate and EDTA during synthesis of the CeNPs seemed to create a more durable stabilizer and allowed the CeNPs to evade active removal by cells of the immune system. In the future, establishing bioequivalence profiles among nanoparticle formulations would be prudent given the potential differences in calculated plasma half-life arising from the type of modeling used by different investigators (e.g., compartmental vs noncompartmental). We used a noncompartmental analysis since it appeared to fit the data well, has fewer assumptions than the compartmental models, and has been used to evaluate the pharmacokinetics of other nanoparticles.<sup>54–56</sup>

The differences in nanoceria tissue clearance could reflect either the physical or chemical features of the particle. Nanoparticle size/surface area and charge play a role in cellular uptake of liposomes, polymer nanoparticles, artificial viruses (DNA coated glycocluster nanoparticles) and inorganic nanostructures.<sup>57–60</sup> Once the material is inside the cell, cellular clearance may be influenced by the type of cell the material is sequestered in (i.e., resident tissue macrophages or other organotypic cells), the subcellular location of the nanoparticles, and natural degradation processes. We have not yet examined these possibilities for these custom CeNPs, but having a better understanding of the cycle of cellular uptake and clearance is a critical requirement for the therapeutic development of nanomaterials, especially since the patterns of tissue deposition and clearance appear to vary significantly among different species and different strains within species.

Previous studies examining nanoceria deposition in the brain following intravenous administration have been inconclusive: brain ceria content was very low.<sup>31,32,35,53</sup> The brain deposition of the CeNPs in the current study was dose-dependent and significantly higher than that observed in other studies, even when normalized to the nanoceria dose.<sup>27,29,31,32</sup> TEM images from brains of animals with EAE indicate that our CeNPs were widely distributed within cells of the cerebellum and were not simply taken up by endothelial cells (Figure 6B). Moreover, the cumulative CeNP dose correlated well with biological action (Figure 5B), which is consistent with regional pathological effects of EAE within the brain. Similar brain ceria content was measured in both the EAE and healthy mice treated

with the same doses of CeNPs, which suggests that our CeNP formulation may cross the normal BBB (Figures 2D and 6A). Since the tight junctions of the BBB exceed the size of our particles (4–20 nm), it is possible that some of the CeNPs may have entered the brain *via* paracellular or transcellular transport processes. Alternatively, adsorption of plasma proteins such as ApoE or albumin may facilitate movement of CeNPs into tissues such as the brain, or the CeNPs may enter the brain by selective transport mechanisms. Resolving this question will require further study.

The amount of CeNPs deposited in the brain was similar to other metal oxide nanomaterials (Au, Pt, and Ti) that have either bypassed the BBB *via* intranasal delivery or have been engineered to use endogenous, selective BBB transport mechanisms to improve brain deposition.<sup>61–64</sup> We hypothesize that the unique protein corona formed around these citrate-EDTA stabilized CeNPs is responsible for their organ deposition pattern, as such protein interactions are among the most important factors influencing biodistribution.<sup>65,66</sup> We may be able to increase brain deposition of our CeNPs by functionalizing the surface with peptide moieties using approaches described by others.<sup>67</sup>

CeNPs are an extremely powerful superoxide dismutase mimetic; 1  $\mu$ g/mL of CeNPs is equivalent to 520 U of SOD.<sup>68,69</sup> Compared to other, non-nanomaterial antioxidants currently under development, CeNPs are unsurpassed in their ability to neutralize free radicals, while their 'durability' and regenerative catalytic capacity allow infrequent dosing compared to other drugs.<sup>70–74</sup> This type of antioxidant activity was preserved *in vivo*, as shown by the reduced ROS levels in the cerebellum of CeNP-treated mice (Figure 7A). The decreased ROS levels appear to be physiologically relevant in that these animals with the MOG<sub>35–55</sub>-induced, chronic progressive model of EAE also exhibited decreased disease symptoms and preserved motor function (Figures 3 and 4). In fact, the amount of CeNPs delivered to the brain correlated with the decrease in cumulative disease severity, represented by the AUC analysis (Figure 5B).

The efficacy of CeNPs depended on the dose given and the timing of treatment initiation. For example, disease onset was significantly delayed only at higher CeNP doses when the CeNPs were given before or shortly after EAE induction, illustrating that higher individual and cumulative doses and an earlier start to treatment were needed to mitigate disease severity most effectively. The highest CeNP dose tested (30 mg/kg, preventative regimen) even demonstrated similar efficacy as fingolimod therapy, though fingolimod was capable of delaying disease onset even when delivered 7 days after EAE induction. This comparison is confounded by the frequency of dosing (intermittent for CeNPs and continuous in the drinking water for fingolimod) and by the fact that CeNP dosing regimens

that started later (day 3 or 7) also resulted in lower cumulative doses of CeNPs. Therapeutic administration of greater CeNP doses starting at 7 days after induction of EAE might have matched the benefit of fingolimod started after EAE induction if higher cumulative doses of CeNP had been given (and preliminary data from our lab indicates that larger cumulative doses of CeNP given after EAE induction can match or exceed the efficacy of fingolimod in EAE).

CeNPs may have to be present at the time of inflammatory cell entry into the CNS at some threshold concentration in order to reduce the levels of ROS in this disease model. The graduated, serial dosing regimens used in these studies may not reach this putative threshold level of activity until later in the experiment. Consistent with such a hypothesis, clinical severity during the latter phase of disease (days 32–35) was significantly reduced at most CeNP doses compared to control treatment ( $p \leq 0.045$ ). Moreover, even starting the 30 mg/kg dose 7 days after EAE induction reduced disease severity (Figure 3), and in this late phase, symptom severity was not different between preventative treatment, fingolimod treatment and the 7 day delay 30 mg/kg treatment groups ( $p > 0.05$ ) (Figure 3D). Last, it is possible that ROS play an important role in the formation of the MOG<sub>35–55</sub> model of EAE. Therefore, the beneficial effects of CeNPs may arise by preventing full expression of the disease model. To the extent this is true, the response to CeNPs may be disease model specific. The late beneficial effects of therapeutic CeNP regimens argue against this line of reasoning since the therapeutic dose schedules allowed full development of the EAE model, but still reduced disease severity late in the illness. Moreover, we conducted studies of a relapsing model of EAE induced by immunization with a different proteolipid protein (PLP<sub>139–151</sub>), and treatment with CeNPs effectively mitigated symptoms in this model as well.<sup>75</sup> Regardless of the timing of CeNP administration relative to disease onset, the cumulative damage was significantly reduced as the CeNPs accumulated and the capacity for ROS neutralization increased.

Specific tests of motor function were also better preserved in the CeNP and fingolimod treated animals, demonstrating a similar dose-dependent effect as that observed with clinical disease scores. In general, we expected CeNPs to improve rostral motor function more than caudal motor function, where the extent of neuropathology is greater. There was a trend in this direction: higher CeNP doses and earlier initiation of treatment tended to preserve function on the hanging wire test, while lower CeNP doses and delayed treatment were associated with greater loss of rostral motor function. However, these trends were not as prominent as we had expected, implying that the neuropathology of EAE in our studies seemed to reflect more equal loss of both caudal and rostral motor function. By the same

token, however, CeNPs improved both caudal and rostral motor function, especially at higher doses and when given at the time of EAE induction.

Fingolimod and ceria nanoparticles have distinct mechanisms of action. Fingolimod interferes with immune cell infiltration into the brain, induces signaling events through sphingosine-1-phosphate receptors and modulates glial reactivity.<sup>76,77</sup> Since migration of activated T cells to their target sites typically takes approximately 7 days, administration of fingolimod within 7 days of EAE induction could still block the majority of T cell infiltration and, thus, T cell mediated pathology. In contrast, ROS levels were significantly lower in cerebellar brain slices of CeNP-treated EAE animals compared to brain slices in fingolimod treated animals. We infer from this that the antioxidant properties of the CeNPs were at least partially responsible for the therapeutic effects of the CeNPs. The clinical disease severity was similar in the CeNP and fingolimod treated animals. Therefore, the differences in ROS levels between CeNP-treated animals and fingolimod treated animals reflect the action of the CeNPs late in the disease rather than any differences in disease severity. Fingolimod may decrease ROS levels earlier in the disease by reducing infiltration of inflammatory cells and ROS production. The antioxidant effect of CeNPs occurs mechanistically downstream from the infiltration of inflammatory cells and may be inadequate to neutralize the levels of ROS generated by the early inflammatory events of EAE when either CeNP therapy is started later or smaller doses of CeNPs are given. In any event, low levels of ROS measured in the *late* phase of disease highlight the unique and durable mechanism of the CeNPs compared to fingolimod.

CeNPs did not alter levels of T cells or macrophages present in the brains of EAE animals (Figure 8), suggesting that CeNPs do not impair immune cell entry into the CNS. The immune cell infiltration studies were conducted at the lowest tested dose of CeNPs (10 mg/kg), which showed relatively modest protective effects. It is possible that some alteration in CNS infiltration of immune cells could be induced by a higher CeNP dose (*i.e.*, 30 mg/kg); however, further analysis of the kinetics of immune cell infiltration, including phenotype and the polarity of T helper cells, is needed before a more definitive conclusion can be made about any immunomodulatory properties of CeNPs.

## MATERIALS/METHODS

**Synthesis and Morphology of CeNPs.** Aqueous 20–30% NH<sub>4</sub>OH was added under high speed mixing to a heated water bath reactor (70 °C) containing ethylenediaminetetraacetic acid (EDTA) and citric acid for stabilization. Aqueous solutions of Ce

While naturally occurring and synthetic antioxidant therapies have shown some efficacy in similar models of EAE, decreasing clinical scores 30–70%,<sup>70–73</sup> the efficacy of such antioxidant therapies is contingent upon several factors.<sup>78</sup> First, the reagent must be able to cross the BBB and localize not only to affected tissues, but also individual cells with a high ROS load. Second, the compound must accumulate in the brain at a high enough concentration to be clinically effective in the treatment of disease. Last, the therapeutic agent must have a half-life in tissue sufficient to inhibit ROS levels long enough to have an appreciable effect on disease progression/symptoms and must retain sufficient catalytic activity to neutralize excessive amounts of ROS produced as part of the disease process. Given that the majority of patients with MS eventually convert to the chronic, progressive form of MS, the likelihood and necessity of long-term treatment is high, and a less frequent dosing regimen is desirable. In this study, the effectiveness of the relatively infrequent dosing regimen was made possible by the long half-life of cerium oxide, the cumulative effect of repeated doses and the durability of the regenerative, catalytic, antioxidant activity of CeNPs.

## CONCLUSION

This is the first report to demonstrate efficacy of cerium oxide nanoparticles in the treatment of a well-characterized, autoimmune, neurodegenerative disease model in intact animals. Most of the therapeutic potential of commercial cerium oxide nanoparticles has been assessed using *in vitro* or cell culture models<sup>6,24,26</sup> or *in vivo* in models with no clear clinical correlate.<sup>27</sup> Nevertheless, CeNPs have reduced retinal damage,<sup>1</sup> reduced the size of infarcts in a middle cerebral artery model of ischemia in rodents,<sup>2</sup> and improved cardiac function in a murine model of cardiomyopathy.<sup>28</sup> In all of these studies, the beneficial effects of cerium oxide nanoparticles have been attributed to the antioxidant activity of the particles. In the current study, CeNPs mitigated the severity of EAE in mice, as indicated by reduced disease severity scores and preserved motor function. Thus, CeNPs are novel synthetic antioxidant catalysts with measurable CNS penetrance, prolonged retention in the CNS, and high, regenerative catalytic activity that hold great promise for use in MS patients and, potentially, other ROS-mediated disorders of the CNS.

(NO<sub>3</sub>)<sub>3</sub>·6H<sub>2</sub>O were added under high speed mixing. Next, a 50% H<sub>2</sub>O<sub>2</sub> solution was added to the vessel and mixed with a high speed shearing mixer at 5500 rpm. The reactor temperature was raised to 80 °C and held at this temperature for 60 min. The reaction was cooled to room temperature overnight and diafiltrated to remove excess free ions with a Millipore, cellulose

regenerated column to a pH of 7.2 and conductivity less than 10 mS. Particle size and composition were confirmed *via* electron diffraction (ED), X-ray diffraction (XRD), dynamic light scattering (DLS) and transmission electron microscope (TEM). The combination of EDTA and citrate prevented aggregation more effectively than either agent alone, and particles stabilized only with EDTA did not exhibit significant neuroprotective effects when tested in our *in vitro* brain slice assay.<sup>4</sup>

**X-ray Diffraction (XRD) Analysis.** The stock CeNP solutions were concentrated, placed onto a zero background quartz disk, allowed to dry under a heat lamp, and then dried in an oven for four hours at 80 °C in vacuum. The solid sample on quartz was analyzed by XRD in a N<sub>2</sub> dry cell attachment. The sample was analyzed for crystallite size in the CeO<sub>2</sub> (220) direction, determined using the Scherrer technique.

**Dynamic Light Scattering (DLS).** The CeNP stock solution (73 mM) was filtered (0.22 μm), and the particle size was determined using a Brookhaven DLS Instrument.

**Electron Diffraction.** Selected-area diffraction patterns were imaged with a 100 μm diameter aperture and a camera length of 55 cm. The camera length was calibrated using an Al polycrystalline standard. The radii of diffraction rings were determined using the radial profile plug-in in Image J software.

**CeNP Aggregation Assay.** CeNPs were placed in simulated body fluid (SBF): 140 mM NaCl, 5 mM KCl, 4 mM NaHCO<sub>3</sub>, 2.5 mM CaCl<sub>2</sub>, 1.5 mM MgSO<sub>4</sub>, 10 mM Na-Hepes (pH: 7.25). DLS analysis was used to assess particle size at various time points.

**CeNP Half-Life.** Three Sprague–Dawley rats (~200 g body weight) received a single, 10 mg/kg intravenous injection of CeNPs, and blood was drawn periodically from the lateral tail vein. Ceria content from the blood collected at each time point was measured using ICP-MS. Plasma half-life was calculated with a noncompartmental analysis model based on WinNonlin, a pharmacokinetic analysis program.

**Clearance of CeNPs from Healthy Mice.** Female SJL/J mice were purchased from Jackson Laboratories and used at 8–10 weeks of age. CeNPs were delivered intravenously at 20 mg/kg on day 0. Animals were euthanized and transcardially perfused with phosphate buffered saline (PBS) before organs were harvested at the following time points: 24 h, 1 month, 2 months, 3 months, 4 months, and 5 months. Cerium content was measured by ICP-MS.

**Induction of EAE in Mice.** All protocols involving animals were approved by the St. Lawrence University Institutional Animal Care and Use Committee (IACUC). Female C57BL/6 mice were purchased from Jackson Laboratories and maintained in our animal facility. Chronic progressive EAE was induced in 8–10 week old mice on day 0 by subcutaneous injection of a homogenized mixture of 200 μg MOG<sub>35–55</sub> peptide (Genscript, Piscataway, NJ) in 50 μL of PBS with 50 μL of incomplete Freund's adjuvant (Sigma Aldrich, St. Louis, MO) containing 4 mg/ml *Mycobacterium tuberculosis* H37Ra (BD Diagnostic Systems, Sparks, MD). An intraperitoneal injection of 200 ng of pertussis toxin (List Biological Laboratories, Campbell CA) in 100 μL of PBS was also delivered on days 0 and 2.

**CeNP and Fingolimod Administration.** CeNPs were administered to the mice in a sterile, sodium citrate buffer (70 mM NaCl, 70 mM Na-citrate, 10 mM Na-Hepes, pH 7.4; 100 μL injection volume), and this solution alone was used for control injections. CeNPs were administered intravenously in one of three regimens: preventative, therapeutic-3 day delay, or therapeutic-7 day delay. The preventative group received CeNPs starting one day before disease induction, on the day of induction, on day 3 and then at set intervals after induction (see Table 1), whereas the therapeutic groups received the drug starting either 3 or 7 days after induction of EAE. Fingolimod (Cayman Chemical, Ann Arbor, MI) was prepared fresh daily and given in the drinking water (2 μg/L) beginning on day 7.

**Clinical Scoring.** Disease severity was rated twice daily, independently by two or more observers. Clinical scores were assigned as follows: 0, normal tail tone and limb movement; 0.5, tail drags when walking, but can still curl around observer's finger; 1, tail has no tone or curl and drags when animal walks; 2, impaired or clumsy gait; 2.5, partial paralysis of one or both hind limbs; 3, complete paralysis of one hind limb; 3.5, complete paralysis of both hind limbs; 4, partial or complete paralysis of

one or both front limbs; 5, moribund. Any mouse with a clinical score ≥ 4 or a clinical score of 3.5 and an inability to groom itself for greater than 5 days was euthanized. Two or three investigators were involved in the clinical scoring, and the diversity of clinical scores among the investigators was less than 15%. As a measure of cumulative disease severity, the area under the curve (AUC) of daily clinical scores was calculated for each animal. Clinical scores wax and wane in EAE, and the area under the curve is less sensitive to day-to-day variations in clinical scores and provides a sensitive index of disease severity over the entire time course of the disease.<sup>79</sup> The AUC of the clinical score for each animal and the means between the treatment groups were compared. The onset of illness was defined as the postimmunization day preceding two successive days on which the clinical scores increased by ≥20%. Estimates for disease severity during the chronic phase of the disease were calculated by averaging the clinical scores of the last four days of the experiment (days 32–35).

**Tests of Motor Function.** For the rotarod test, each mouse was placed onto a drum (Med Associates, St. Albans, VT) rotating at 28 rpm, and the latency to fall from the drum (300 s, maximum) was measured. In the hanging wire task, each mouse was placed in an open-top Plexiglas box with a steel wire, grid floor. The box was turned upside down 60 cm above the counter top, and the latency to fall was measured. The balance beam apparatus consisted of a 28 mm square beam (100 cm in length and elevated 50 cm above the counter top) that led to a 20 cm × 20 cm dark enclosure. A 60 W light bulb illuminated the open end of the beam and motivated the mice to traverse the beam and reach the dark goal box. Each mouse was placed on the illuminated end of the beam and given up to 60 s to reach the dark, goal box. Balance and gait quality were scored using a 5 point scale (5 = normal gait to 0 = falls off beam immediately). For all tasks, each animal was trained for 5 days before EAE induction. After induction, tests were performed daily for the duration of the experiment.

**Biodistribution of CeNPs in EAE Mice.** EAE mice were euthanized by isoflurane overdose and transcardially perfused with PBS, and organs were removed to analyze tissue-specific ceria content. The dissection tools were cleaned between each animal to decrease cross contamination with ceria. Tissues were frozen and analyzed by ICP-MS at the Trace Metal and Analytics facility at Dartmouth College. Organ samples (50–100 mg) were immersed in HNO<sub>3</sub> and heated at 105 °C for 45 min and allowed to cool. After cooling was achieved, deionized water was added to each sample tube to achieve a final acid content of 5%.

**TEM Analysis.** Tissue samples for TEM analysis were fixed in glutaraldehyde and osmium tetroxide, then treated with successively higher ratios of ethanol/water and finally immersed in 100% acetone. These dehydrated samples were immersed in 3/1 acetone/Embed 812 for 12 h, 1/1 acetone/embed 812 for 4 h, 3/1 acetone/Embed 812 for 4 h, and finally 100% Embed 812 for 12 h. Last, each sample was cured at 60 °C for 12 h. Thin sections (70 nm) of the epoxy-embedded tissue were prepared with an ultramicrotome and transferred to lacey-carbon covered, copper TEM grids. The sections were imaged at 100 kV using a JEOL 100CX II transmission electron microscope.

**Preparation of Brain Slices for ROS Detection.** Beginning one week after behavioral testing and drug therapy had ended (post-induction day 42), mice exhibiting the most severe clinical symptoms in each group were sacrificed by rapid decapitation. Brains were quickly removed and placed in a chilled, choline-based slicing solution before 400 μm thick transverse cerebellar slices were cut along a rostral to caudal axis (−5.68 to −6.84 mm Bregma) using a vibratome.<sup>22</sup> The samples were allowed to recover for 1 h in control, artificial cerebral spinal fluid (aCSF) and bubbled with 5% CO<sub>2</sub>, 95% O<sub>2</sub> gas (pH 7.4, 300 mOsm). For each ROS measurement, two sets of anatomically matched brain slices were taken from EAE animals, one from a control animal and the other from either a CeNP or a fingolimod treated animal. The CeNP and fingolimod treated animals were also matched on their peak clinical scores.

**Measurement of Reactive Oxygen/Nitrogen Species in Brain Slices.** Brain slices were loaded with 20 μM 5-chloromethyl-2',7'-dichlorodihydro-fluorescein diacetate (CM-H<sub>2</sub>DCFDA; Invitrogen

Grand Island, NY) dissolved in DMSO and added to the aCSF perfusate for 20–30 min at 37 °C and then washed for 10 min in Hibernate A low fluorescence solution (Brain Bits, LLC, Springfield, IL). After a washing step, the sections were mounted on a coverslip with Hibernate A and visualized with a Nikon TE 2000-U microscope (Nikon Instruments Melville, NY). Sequential images were collected in a randomized order using a 4× Plan Fluor objective (Nikon Instruments) under identical conditions (*i.e.*, light intensity, exposure time, camera acquisition settings). Fluorescence was measured by briefly (~300 ms) exciting the tissue at 480 ± 40 nm. Emitted fluorescence (535 ± 50 nm) from the probe was filtered using a 505 nm, long-pass, dichroic mirror (Chroma Technology Bennington, VT), intensified and measured with a cooled CCD gain EM camera (Hamamatsu CCD EM C9100; Bridgewater, NJ). These exposure times did not induce photo-oxidation in the sections even after repeated image capture. The digital images were acquired and processed with Compix SimplePCI 6.0 software (C Imaging Systems Cranberry Township, PA). Four images were captured, the total gray level for each was calculated, and the light intensities were summed to determine a total gray level for the section. Results were expressed as the ratio of the fluorescence in each test condition to fluorescence in the matched control slice imaged at the same time point within the experimental sequence.

**Microvasculature Staining and Visualization.** Alternatively, live brain sections (prepared as described above) were stained with mouse anti-laminin conjugated to Alexa Fluor 488 (EMD Millipore; 1:100) for 1 h in aCSF. Tissue was washed twice in low fluorescence Hibernate A at room temperature (15 min each wash; Brain Bits, Springfield, IL). Sections were mounted on a coverslip with a drop of Hibernate A, and microvasculature was visualized using epifluorescence microscopy as described for CM-H<sub>2</sub>DCFDA visualization.

**CNS Cellular Infiltration.** On day 45, 10 days after clinical testing and drug therapy had ended, mice that were treated with 10 mg/kg CeNPs or vehicle alone were euthanized by isoflurane overdose prior to transcardial perfusion with PBS. Brain and spinal cord tissues were harvested and homogenized, and lymphocytes were isolated using Percoll gradient separation (GE Healthcare, Pittsburgh, PA). Any red blood cells remaining among the isolated lymphocytes were lysed by exposure to hypotonic conditions. The remaining lymphocytes were stained with anti-CD4 PE (eBioscience, San Diego CA), anti-CD11b PerCp (BioLegend, San Diego CA), and anti-CD45 PE (BioLegend) antibodies and fixed with 4% paraformaldehyde for flow cytometry analysis. Samples were analyzed at the Wistar Institute (Philadelphia, PA), and data analysis was performed using the FCS Express program (De Novo Software, Los Angeles, CA).

**Statistical Analysis.** For statistical analysis, the area under the curve was calculated for clinical scores and for motor tests by summing the daily scores to generate cumulative disease severity measurements. For ordinal data (clinical scores and balance beam), Friedman's test for nonparametric, multiple comparisons was used to evaluate main effects, and Dunn's post-hoc test (one-tailed) was used to compare treatment groups to control. Day-by-day comparisons and other comparisons used Wilcoxon's signed rank test (one-tailed). Rotarod and hanging wire data were analyzed using a repeated measures ANOVA to test for main effects, and Dunn's test (one-tailed) was used for post-hoc tests when the ANOVA indicated that significant differences existed among treatment groups. A repeated measures design to test for main effects was used to assess dose–responses for clinical scores and motor testing used, and the Holm–Sidak method was used for post-hoc analysis. For statistical analysis of sections labeled with the fluorescent, free radical probe, raw fluorescence values were compared using a factorial ANOVA and Dunnett's post-hoc analysis.

**Conflict of Interest:** The authors declare the following competing financial interest(s): Drs. Ana Estevez, William DeCoteau, Joseph Erlichman, and Kenneth Reed have equity ownership that exceeds 5% in Cerion NRx which funded a portion of this work.

## REFERENCES AND NOTES

- Kong, L.; Cai, X.; Zhou, X.; Wong, L. L.; Karakoti, A. S.; Seal, S.; McGinnis, J. F. Nanoceria Extend Photoreceptor Cell Lifespan in Tubby Mice by Modulation of Apoptosis/Survival Signaling Pathways. *Neurobiol. Dis.* **2011**, *42*, 514–523.
- Kim, C. K.; Kim, T.; Choi, I. Y.; Soh, M.; Kim, D.; Kim, Y. J.; Jang, H.; Yang, H. S.; Kim, J. Y.; Park, H. K.; *et al.* Ceria Nanoparticles That Can Protect against Ischemic Stroke. *Angew. Chem., Int. Ed.* **2012**, *51*, 11039–11043.
- Andreescu, A.; Ornatska, M.; Erlichman, J. S.; Estevez, A. Y.; Leiter, J. C. Biomedical Applications of Metal Oxide Nanoparticles. In *Fine Particles in Medicine and Pharmacy*; Matijević, E., Ed.; Springer Science+Business Media, LLC: New York, 2012; pp 57–100.
- Estevez, A. Y.; Erlichman, J. S. Cerium Oxide Nanoparticles for the Treatment of Neurological Oxidative Stress Diseases. In *Oxidative Stress: Diagnostics, Prevention, and Therapy*; Andreescu, S., Ed.; American Chemical Society: Washington, DC, 2011; pp 255–288.
- Tarnuzzer, R. W.; Colon, J.; Patil, S.; Seal, S. Vacancy Engineered Ceria Nanostructures for Protection from Radiation-Induced Cellular Damage. *Nano Lett.* **2005**, *5*, 2573–2577.
- Schubert, D.; Dargusch, R.; Raitano, J.; Chan, S.-W. Cerium and Yttrium Oxide Nanoparticles Are Neuroprotective. *Biochem. Biophys. Res. Commun.* **2006**, *342*, 86–91.
- Colon, J.; Herrera, L.; Smith, J.; Patil, S.; Komanski, C.; Kupelian, P.; Seal, S.; Jenkins, D. W.; Baker, C. H. Protection from Radiation-Induced Pneumonitis Using Cerium Oxide Nanoparticles. *Nanomedicine* **2009**, *5*, 225–231.
- Campbell, C. T.; Peden, C. H. Oxygen Vacancies and Catalysis on Ceria Surfaces. *Science* **2005**, *309*, 713–714.
- Zhang, H. Z.; Chen, B.; Ren, Y.; Waychunas, G. A.; Banfield, J. F. Response of Nanoparticle Structure to Different Types of Surface Environments: Wide-Angle X-Ray Scattering and Molecular Dynamics Simulations. *Phys. Rev. B* **2010**, *81*, 125444.
- Trovarelli, A. Structural and Oxygen Storage/Release Properties of CeO<sub>2</sub>-Based Solid Solutions. *Comments Inorg. Chem.* **1999**, *20*, 263–284.
- Schallow, T.; Laurin, M.; Brandt, B.; Schauermann, S.; Guimond, S.; Kuhlenbeck, H.; Starr, D. E.; Shaikhutdinov, S. K.; Libuda, J.; Freund, H. J. Oxygen Storage at the Metal/Oxide Interface of Catalyst Nanoparticles. *Angew. Chem., Int. Ed.* **2005**, *44*, 7601–7605.
- Dutta, P.; Pal, S.; Seehra, M. S.; Shi, Y.; Eyring, E. M.; Ernst, R. D. Concentration of Ce<sup>3+</sup> and Oxygen Vacancies in Cerium Oxide Nanoparticles. *Chem. Mater.* **2006**, *18*, 5144–5146.
- Sayle, T. X.; Molinari, M.; Das, S.; Bhatta, U. M.; Mobus, G.; Parker, S. C.; Seal, S.; Sayle, D. C. Environment-Mediated Structure, Surface Redox Activity and Reactivity of Ceria Nanoparticles. *Nanoscale* **2013**, *5*, 6063–6073.
- Chen, J.; Patil, S.; Seal, S.; McGinnis, J. F. Rare Earth Nanoparticles Prevent Retinal Degeneration Induced by Intracellular Peroxides. *Nat. Nanotechnol.* **2006**, *1*, 142–150.
- Wong, L. L.; Hirst, S. M.; Pye, Q. N.; Reilly, C. M.; Seal, S.; McGinnis, J. F. Catalytic Nanoceria Are Preferentially Retained in the Rat Retina and Are Not Cytotoxic after Intravitreal Injection. *PLoS One* **2013**, *8*, e58431.
- Das, S.; Singh, S.; Dowding, J. M.; Oommen, S.; Kumar, A.; Sayle, T. X.; Saraf, S.; Patra, C. R.; Vlahakis, N. E.; Sayle, D. C.; *et al.* The Induction of Angiogenesis by Cerium Oxide Nanoparticles through the Modulation of Oxygen in Intracellular Environments. *Biomaterials* **2012**, *33*, 7746–7755.
- Dowding, J. M.; Dosani, T.; Kumar, A.; Seal, S.; Self, W. T. Cerium Oxide Nanoparticles Scavenge Nitric Oxide Radical (NO). *Chem. Commun.* **2012**, *48*, 4896–4898.
- Zhou, X. H.; Wong, L. L.; Karakoti, A. S.; Seal, S.; McGinnis, J. F. Nanoceria Inhibit the Development and Promote the Regression of Pathologic Retinal Neovascularization in the Vldlr Knockout Mouse. *PLoS One* **2011**, *6*, e16733.
- Cimini, A.; D'Angelo, B.; Das, S.; Gentile, R.; Benedetti, E.; Singh, V.; Monaco, A. M.; Santucci, S.; Seal, S.

Antibody-Conjugated Pegylated Cerium Oxide Nanoparticles for Specific Targeting of Abeta Aggregates Modulate Neuronal Survival Pathways. *Acta Biomater.* **2012**, *8*, 2056–2067.

20. Karakoti, A.; Singh, S.; Dowding, J. M.; Seal, S.; Self, W. T. Redox-Active Radical Scavenging Nanomaterials. *Chem. Soc. Rev.* **2010**, *39*, 4422–4432.

21. Bhargava, N.; Das, M.; Karakoti, A. S.; Patil, S.; Kang, J. F.; Stancescu, M.; Kindy, M. S.; Seal, S.; Hickman, J. J. Regeneration of Adult Mice Motoneurons Utilizing a Defined System and Anti-Oxidant Nanoparticle. *J. Nanoneurosci.* **2009**, *1*, 130–143.

22. Estevez, A. Y.; Pritchard, S.; Harper, K.; Aston, J. W.; Lynch, A.; Lucky, J. J.; Ludington, J. S.; Chatani, P.; Mosenthal, W. P.; Leiter, J. C.; *et al.* Neuroprotective Mechanisms of Cerium Oxide Nanoparticles in a Mouse Hippocampal Brain Slice Model of Ischemia. *Free Radical Biol. Med.* **2011**, *51*, 1155–1163.

23. Cohen, C. A.; Kurnick, M. D.; Rzagalinski, B. A. Cerium Oxide Nanoparticles Extend Lifespan and Protect *Drosophila Melanogaster* from Paraquat (Pq)-Induced Oxidative Stress (Os). *Free Radical Biol. Med.* **2006**, *41*, S20–S20.

24. Rzagalinski, B. A.; Meehan, K.; Davis, R. M.; Xu, Y.; Miles, W. C.; Cohen, C. A. Radical Nanomedicine. *Nanomedicine (London, U.K.)* **2006**, *1*, 399–412.

25. Silva, G. A. Seeing the Benefits of Ceria. *Nat. Nanotechnol.* **2006**, *1*, 92–94.

26. Das, M.; Patil, S.; Bhargava, N.; Kang, J.-F.; Riedel, L. M.; Seal, S.; Hickman, J. J. Auto-Catalytic Ceria Nanoparticles Offer Neuroprotection to Adult Rat Spinal Cord Neurons. *Biomaterials* **2007**, *28*, 1918–1925.

27. Hirst, S. M.; Karakoti, A. S.; Singh, S.; Self, W.; Tyler, R. D.; Seal, S.; Reilly, C. M. Bio-Distribution and *in Vivo* Antioxidant Effects of Cerium Oxide Nanoparticles in Mice. *Environ. Toxicol.* **2011**, *28*, 107–118.

28. Niu, J.; Azfer, A.; Rogers, L. M.; Wang, X.; Kolattukudy, P. E. Cardioprotective Effects of Cerium Oxide Nanoparticles in a Transgenic Murine Model of Cardiomyopathy. *Cardiovasc. Res.* **2007**, *73*, 549–559.

29. Yokel, R. A.; Au, T. C.; MacPhail, R.; Hardas, S. S.; Butterfield, D. A.; Sultana, R.; Goodman, M.; Tseng, M. T.; Dan, M.; Haghnaz, H.; *et al.* Distribution, Elimination, and Bio-persistence to 90 Days of a Systemically Introduced 30 nm Ceria-Engineered Nanomaterial in Rats. *Toxicol. Sci.* **2012**, *127*, 256–268.

30. Yokel, R. A.; Florence, R. L.; Unrine, J. M.; Tseng, M. T.; Graham, U. M.; Wu, P. Y. K.; Grulke, E. A.; Sultana, R.; Hardas, S. S.; Butterfield, D. A. Biodistribution and Oxidative Stress Effects of a Systematically-Introduced Commercial Ceria Engineered Nanomaterial. *Nanotoxicology* **2009**, *3*, 234–248.

31. Hardas, S. S.; Butterfield, D. A.; Sultana, R.; Tseng, M. T.; Dan, M.; Florence, R. L.; Unrine, J. M.; Graham, U. M.; Wu, P.; Grulke, E. A.; *et al.* Brain Distribution and Toxicological Evaluation of a Systemically Delivered Engineered Nanoscale Ceria. *Toxicol. Sci.* **2010**, *116*, 562–576.

32. Hardas, S. S.; Sultana, R.; Warrier, G.; Dan, M.; Florence, R. L.; Wu, P.; Grulke, E. A.; Tseng, M. T.; Unrine, J. M.; Graham, U. M.; *et al.* Rat Brain Pro-Oxidant Effects of Peripherally Administered 5 nm Ceria 30 Days after Exposure. *Neurotoxicology* **2012**, *33*, 1147–1155.

33. Nalabotu, S. K.; Kolli, M. B.; Triest, W. E.; Ma, J. Y.; Manne, N. D.; Katta, A.; Addagarla, H. S.; Rice, K. M.; Blough, E. R. Intratracheal Instillation of Cerium Oxide Nanoparticles Induces Hepatic Toxicity in Male Sprague-Dawley Rats. *Int. J. Nanomed.* **2011**, *6*, 2327–2335.

34. Tseng, M. T.; Lu, X.; Duan, X.; Hardas, S. S.; Sultana, R.; Wu, P.; Unrine, J. M.; Graham, U.; Butterfield, D. A.; Grulke, E. A.; *et al.* Alteration of Hepatic Structure and Oxidative Stress Induced by Intravenous Nanoceria. *Toxicol. Appl. Pharmacol.* **2012**, *260*, 173–182.

35. Sousa, F.; Mandal, S.; Garrovo, C.; Astolfo, A.; Bonifacio, A.; Latawiec, D.; Menk, R. H.; Arfelli, F.; Huewel, S.; Legname, G.; *et al.* Functionalized Gold Nanoparticles: A Detailed *in Vivo* Multimodal Microscopic Brain Distribution Study. *Nanoscale* **2010**, *2*, 2826–2834.

36. Dowding, J. M.; Das, S.; Kumar, A.; Dosani, T.; McCormack, R.; Gupta, A.; Sayle, T. X.; Sayle, D. C.; von Kalm, L.; Seal, S.; *et al.* Cellular Interaction and Toxicity Depend on Physicochemical Properties and Surface Modification of Redox-Active Nanomaterials. *ACS Nano* **2013**, *7*, 4855–4868.

37. DiFrancesco, A. G.; Hailstone, R. K.; Langner, A.; Reed, K. J. Method of Preparing Cerium Dioxide Nanoparticles. U.S. Patent Application Publication 2011/0056123.

38. Hemmer, B.; Nessler, S.; Zhou, D.; Kieseier, B.; Hartung, H. P. Immunopathogenesis and Immunotherapy of Multiple Sclerosis. *Nat. Clin. Pract. Neurol.* **2006**, *2*, 201–211.

39. Raivich, G.; Banati, R. Brain Microglia and Blood-Derived Macrophages: Molecular Profiles and Functional Roles in Multiple Sclerosis and Animal Models of Autoimmune Demyelinating Disease. *Brain Res. Brain Res. Rev.* **2004**, *46*, 261–281.

40. Huppert, J.; Closhen, D.; Croxford, A.; White, R.; Kulig, P.; Pietrowski, E.; Bechmann, I.; Becher, B.; Luhmann, H. J.; Waisman, A.; *et al.* Cellular Mechanisms of IL-17-Induced Blood-Brain Barrier Disruption. *FASEB J.* **2010**, *24*, 1023–1034.

41. van Horssen, J.; Witte, M. E.; Schreibelt, G.; de Vries, H. E. Radical Changes in Multiple Sclerosis Pathogenesis. *Biochim. Biophys. Acta* **2011**, *1812*, 141–150.

42. Cohen, J. A.; Barkhof, F.; Comi, G.; Hartung, H. P.; Khatri, B. O.; Montalban, X.; Pelletier, J.; Capra, R.; Gallo, P.; Izquierdo, G.; *et al.* Oral Fingolimod or Intramuscular Interferon for Relapsing Multiple Sclerosis. *N. Engl. J. Med.* **2010**, *362*, 402–415.

43. Ledeboer, A.; Wierinckx, A.; Bol, J. G.; Floris, S.; Renardel de Lavalette, C.; De Vries, H. E.; van den Berg, T. K.; Dijkstra, C. D.; Tilders, F. J.; van dam, A. M. Regional and Temporal Expression Patterns of Interleukin-10, Interleukin-10 Receptor and Adhesion Molecules in the Rat Spinal Cord During Chronic Relapsing EAE. *J. Neuroimmunol.* **2003**, *136*, 94–103.

44. Alusi, S. H.; Worthington, J.; Glickman, S.; Bain, P. G. A Study of Tremor in Multiple Sclerosis. *Brain* **2001**, *124*, 720–730.

45. Dobrovolskaia, M. A.; McNeil, S. E. Immunological Properties of Engineered Nanomaterials. *Nat. Nanotechnol.* **2007**, *2*, 469–478.

46. Vroman, L.; Adams, A. L.; Fischer, G. C.; Munoz, P. C. Interaction of High Molecular Weight Kininogen, Factor XII, and Fibrinogen in Plasma at Interfaces. *Blood* **1980**, *55*, 156–159.

47. Walkey, C. D.; Chan, W. C. Understanding and Controlling the Interaction of Nanomaterials with Proteins in a Physiological Environment. *Chem. Soc. Rev.* **2012**, *41*, 2780–2799.

48. Fischer, H. C.; Chan, W. C. Nanotoxicity: The Growing Need for *in Vivo* Study. *Curr. Opin. Biotechnol.* **2007**, *18*, 565–571.

49. Aggarwal, P.; Hall, J. B.; McLeland, C. B.; Dobrovolskaia, M. A.; McNeil, S. E. Nanoparticle Interaction with Plasma Proteins as It Relates to Particle Biodistribution, Biocompatibility and Therapeutic Efficacy. *Adv. Drug Delivery Rev.* **2009**, *61*, 428–437.

50. Karmali, P. P.; Simberg, D. Interactions of Nanoparticles with Plasma Proteins: Implication on Clearance and Toxicity of Drug Delivery Systems. *Expert Opin. Drug Delivery* **2011**, *8*, 343–357.

51. Walkey, C. D.; Olsen, J. B.; Guo, H.; Emili, A.; Chan, W. C. Nanoparticle Size and Surface Chemistry Determine Serum Protein Adsorption and Macrophage Uptake. *J. Am. Chem. Soc.* **2012**, *134*, 2139–2147.

52. Rodriguez, P. L.; Harada, T.; Christian, D. A.; Pantano, D. A.; Tsai, R. K.; Discher, D. E. Minimal “Self” Peptides That Inhibit Phagocytic Clearance and Enhance Delivery of Nanoparticles. *Science* **2013**, *339*, 971–975.

53. Dan, M.; Tseng, M. T.; Wu, P.; Unrine, J. M.; Grulke, E. A.; Yokel, R. A. Brain Microvascular Endothelial Cell Association and Distribution of a 5 nm Ceria Engineered Nanomaterial. *Int. J. Nanomed.* **2012**, *7*, 4023–4036.

54. Shahnaz, G.; Iqbal, J.; Rahmat, D.; Perera, G.; Laffleur, F.; Rossi, D.; Bernkop-Schnurch, A. Development and *in Vivo* Characterization of a Novel Peptide Drug Delivery System

Providing Extended Plasma Half Life. *J. Controlled Release* **2012**, *157*, 375–382.

55. Arvizu, R. R.; Miranda, O. R.; Moyano, D. F.; Walden, C. A.; Giri, K.; Bhattacharya, R.; Robertson, J. D.; Rotello, V. M.; Reid, J. M.; Mukherjee, P. Modulating Pharmacokinetics, Tumor Uptake and Biodistribution by Engineered Nanoparticles. *PLoS One* **2011**, *6*, e24374.

56. Chu, K. S.; Hasan, W.; Rawal, S.; Walsh, M. D.; Enlow, E. M.; Luft, J. C.; Bridges, A. S.; Kuijer, J. L.; Napier, M. E.; Zamboni, W. C.; et al. Plasma, Tumor and Tissue Pharmacokinetics of Docetaxel Delivered via Nanoparticles of Different Sizes and Shapes in Mice Bearing Skov-3 Human Ovarian Carcinoma Xenograft. *Nanomedicine* **2013**, *9*, 686–693.

57. Rensen, P. C.; Sliedregt, L. A.; Ferns, M.; Kieviet, E.; van Rossenberg, S. M.; van Leeuwen, S. H.; van Berkel, T. J.; Biessen, E. A. Determination of the Upper Size Limit for Uptake and Processing of Ligands by the Asialoglycoprotein Receptor on Hepatocytes *In Vitro* and *In Vivo*. *J. Biol. Chem.* **2001**, *276*, 37577–37584.

58. Win, K. Y.; Feng, S. S. Effects of Particle Size and Surface Coating on Cellular Uptake of Polymeric Nanoparticles for Oral Delivery of Anticancer Drugs. *Biomaterials* **2005**, *26*, 2713–2722.

59. Chithrani, B. D.; Ghazani, A. A.; Chan, W. C. Determining the Size and Shape Dependence of Gold Nanoparticle Uptake into Mammalian Cells. *Nano Lett.* **2006**, *6*, 662–668.

60. Chithrani, B. D.; Chan, W. C. Elucidating the Mechanism of Cellular Uptake and Removal of Protein-Coated Gold Nanoparticles of Different Sizes and Shapes. *Nano Lett.* **2007**, *7*, 1542–1550.

61. Wang, J.; Liu, Y.; Jiao, F.; Lao, F.; Li, W.; Gu, Y.; Li, Y.; Ge, C.; Zhou, G.; Li, B.; et al. Time-Dependent Translocation and Potential Impairment on Central Nervous System by Intranasally Instilled  $\text{TiO}_2$  Nanoparticles. *Toxicology* **2008**, *254*, 82–90.

62. Gan, C. W.; Feng, S. S. Transferrin-Conjugated Nanoparticles of Poly(lactide)-D-alpha-tocopheryl Polyethylene Glycol Succinate Diblock Copolymer for Targeted Drug Delivery across the Blood-Brain Barrier. *Biomaterials* **2010**, *31*, 7748–7757.

63. Lasagna-Reeves, C.; Gonzalez-Romero, D.; Barria, M. A.; Olmedo, I.; Clos, A.; Sadagopa Ramanujam, V. M.; Urayama, A.; Vergara, L.; Kogan, M. J.; Soto, C. Bioaccumulation and Toxicity of Gold Nanoparticles after Repeated Administration in Mice. *Biochem. Biophys. Res. Commun.* **2010**, *393*, 649–655.

64. Takamiya, M.; Miyamoto, Y.; Yamashita, T.; Deguchi, K.; Ohta, Y.; Ikeda, Y.; Matsuura, T.; Abe, K. Neurological and Pathological Improvements of Cerebral Infarction in Mice with Platinum Nanoparticles. *J. Neurosci. Res.* **2011**, *89*, 1125–1133.

65. Dutta, D.; Sundaram, S. K.; Teeguarden, J. G.; Riley, B. J.; Fifield, L. S.; Jacobs, J. M.; Addleman, S. R.; Kaysen, G. A.; Moudgil, B. M.; Weber, T. J. Adsorbed Proteins Influence the Biological Activity and Molecular Targeting of Nanomaterials. *Toxicol. Sci.* **2007**, *100*, 303–315.

66. Luck, M.; Pauke, B. R.; Schroder, W.; Blunk, T.; Muller, R. H. Analysis of Plasma Protein Adsorption on Polymeric Nanoparticles with Different Surface Characteristics. *J. Biomed. Mater. Res., Part A* **1998**, *39*, 478–485.

67. Malhotra, M.; Prakash, S. Targeted Drug Delivery across Blood-Brain-Barrier Using Cell Penetrating Peptides Tagged Nanoparticles. *Curr. Nanosci.* **2011**, *7*, 81–93.

68. Ganesana, M.; Erlichman, J. S.; Andreescu, S. Real-Time Monitoring of Superoxide Accumulation and Antioxidant Activity in a Brain Slice Model Using an Electrochemical Cytochrome C Biosensor. *Free Radical Biol. Med.* **2012**, *53*, 2240–2249.

69. Heckert, E. G.; Karakoti, A. S.; Seal, S.; Self, W. T. The Role of Cerium Oxide Redox State in the SOD Mimetic Activity of Nanoceria. *Biomaterials* **2008**, *29*, 2705–2709.

70. Aktas, O.; Waiczies, S.; Smorodchenko, A.; Dorr, J.; Seeger, B.; Prozorovski, T.; Sallach, S.; Endres, M.; Brocke, S.; Nitsch, R.; et al. Treatment of Relapsing Paralysis in Experimental Encephalomyelitis by Targeting Th1 Cells through Atorvastatin. *J. Exp. Med.* **2003**, *197*, 725–733.

71. Hendriks, J. J.; Alblas, J.; van der Pol, S. M.; van Tol, E. A.; Dijkstra, C. D.; de Vries, H. E. Flavonoids Influence Monocytic GTPase Activity and Are Protective in Experimental Allergic Encephalitis. *J. Exp. Med.* **2004**, *200*, 1667–1672.

72. Moriya, M.; Nakatsuji, Y.; Miyamoto, K.; Okuno, T.; Kinoshita, M.; Kumanogoh, A.; Kusunoki, S.; Sakoda, S. Edaravone, a Free Radical Scavenger, Ameliorates Experimental Autoimmune Encephalomyelitis. *Neurosci. Lett.* **2008**, *440*, 323–326.

73. Stanislaus, R.; Gilg, A. G.; Singh, A. K.; Singh, I. N-Acetyl-L-cysteine Ameliorates the Inflammatory Disease Process in Experimental Autoimmune Encephalomyelitis in Lewis Rats. *J. Autoimmune Dis.* **2005**, *2*, 4.

74. Korsvik, C.; Patil, S.; Seal, S.; Self, W. T. Superoxide Dismutase Mimetic Properties Exhibited by Vacancy Engineered Ceria Nanoparticles. *Chem. Commun. (Cambridge, U.K.)* **2007**, *1056–1058*.

75. DeCouteau, W.; Heckman, K.; Reed, K.; Erlichman, J. S. Ceria Nanoparticles Reduce Disease Severity in a Mouse Model of Multiple Sclerosis. *Nanotechnol.* **2012**, *2012*, *3*, 265–268.

76. Brinkmann, V.; Davis, M. D.; Heise, C. E.; Albert, R.; Cottens, S.; Hof, R.; Bruns, C.; Prieschl, E.; Baumruker, T.; Hiestand, P.; et al. The Immune Modulator FTY720 Targets Sphingosine 1-Phosphate Receptors. *J. Biol. Chem.* **2002**, *277*, 21453–21457.

77. Choi, J. W.; Gardell, S. E.; Herr, D. R.; Rivera, R.; Lee, C. W.; Noguchi, K.; Teo, S. T.; Yung, Y. C.; Lu, M.; Kennedy, G.; et al. FTY720 (Fingolimod) Efficacy in an Animal Model of Multiple Sclerosis Requires Astrocyte Sphingosine 1-Phosphate Receptor 1 (S1P1) Modulation. *Proc. Natl. Acad. Sci. U.S.A.* **2011**, *108*, 751–756.

78. Schreibelt, G.; van Horssen, J.; van Rossum, S.; Dijkstra, C. D.; Drukarch, B.; de Vries, H. E. Therapeutic Potential and Biological Role of Endogenous Antioxidant Enzymes in Multiple Sclerosis Pathology. *Brain Res. Rev.* **2007**, *56*, 322–330.

79. Fleming, K. K.; Bovaird, J. A.; Mosier, M. C.; Emerson, M. R.; LeVine, S. M.; Marquis, J. G. Statistical Analysis of Data from Studies on Experimental Autoimmune Encephalomyelitis. *J. Neuroimmunol.* **2005**, *170*, 71–84.